We would like to thank the reviewers for carefully reading our submitted manuscript and for raising important and insightful questions that helped us improve the quality and readability of the manuscript.

In what fallow below, the comments made by the reviewers are in black and our answers are in red. All changes to the manuscript are marked by "track changes" in the manuscript file.

Anonymous Referee #1

The authors report a photophoretic technique as applied to levitated droplets in a double-ring electrodynamic balance. They show that the droplet position changes slightly when slightly light-absorbing molecules are present in the sample, due to the indirect photophoretic effect. By relating the change in DC balance voltage to the change in position, the authors are able to determine the complex part of the refractive index (cRI). The authors demonstrate the retrieval of the cRI of carminic acid in a PEG400 solution at 0.23 wt% and report agreement within error to their bulk measurements. This is a nice new technique and demonstrates another method that the cRI can be established from measurements on levitated droplets. However, it appears to me that the application of this method to light-absorbing properties of atmospheric sample may be limited. Overall, the paper is well-written and falls within the scope of the journal. Clear answers to the following questions/comments would alleviate my concerns over the applicability of this technique:

1. What range of k is this method appropriate for? An upper and lower limit should be estimated to allow readers to gauge the effectiveness of the method in characterizing brown carbon samples.

There are no theoretical upper and lower limits for retrievals of κ using the described method. On the lower end this would depend on the sensitivity and stability of the experimental set-up. With our system, which could be improved, as mentioned in the manuscript this value is about 10^{-5}. On the upper end of κ values, more energy is absorbed and as a result the signal is generally (not always, see below) stronger and easier to measure. However, this should be compensated with reducing the power of the light source to avoid significant temperature change of the particle.

We chose to emphasize the usefulness of EDB-PPS at the lower range of κ. Because at higher values of κ, other particle phase techniques are available, that are simpler to implement. These include photoacoustic spectroscopy, cavity enhanced spectroscopy, extinction minus scattering and filter based techniques. Therefore one can expect this method to be mostly rewarding at $\kappa \leq 10^{-3}$ in aging experiments that are intended to follow 'bleaching' or 'browning' of BrC.

To better explain the limitations of this technique with regards to a useful range of the imaginary part we added the following figure (figure 7 in the revised manuscript). This figure illustrates the simulated system signal ($\Delta U/U_0$) over 6 orders of magnitude of κ, from 10^{-8} to 10^{-2}, of a 10 μm, PEG400 based particle. At the lower end of this range (left side of figure 7a) κ is effectivity zero and the simulated signal is negative (particle moves away from the light source) due to direct photophoresis (radiation pressure) alone. Note how the signal increases to positive values as κ increases (figure 7a and 7b) due to an increase in the thermal asymmetry parameter. With the increase in κ there more energy that is absorbed on the illuminated side of the particle. This offsets the hotspot of absorbed energy at the 'dark' side of the particle that is due to 'nano-focusing'. As a result, the thermal asymmetry parameter is reduced together with the signal. As

κ continues to increase the asymmetry parameter changes sign from positive to negative as the illuminated side of the particle becomes warmer than the 'dark' side. This is shown in figure 7c as a negative signal and illustrated in 7d as the particle shifts from the regime described by the upper part to the one in the lower part of figure 7d.

Based on this description and on our system's sensitivity limitations we determined the lower limit for κ retrieval at 10^{-5} and do not determine an upper limit. We do however, note areas with high uncertainty, namely, around $\kappa \approx 10^{-3}$, where the change in signal flattens.

An important caveat is the non-injective behavior in figure 7b. To address the issue one would need to understand the order of magnitude of the particle's absorption (for example; is it below or above $\kappa = 10^{-3}$). Additionally, in aging experiments, as κ evolves, the direction of the change of the signal would clarify the direction of the change of κ.

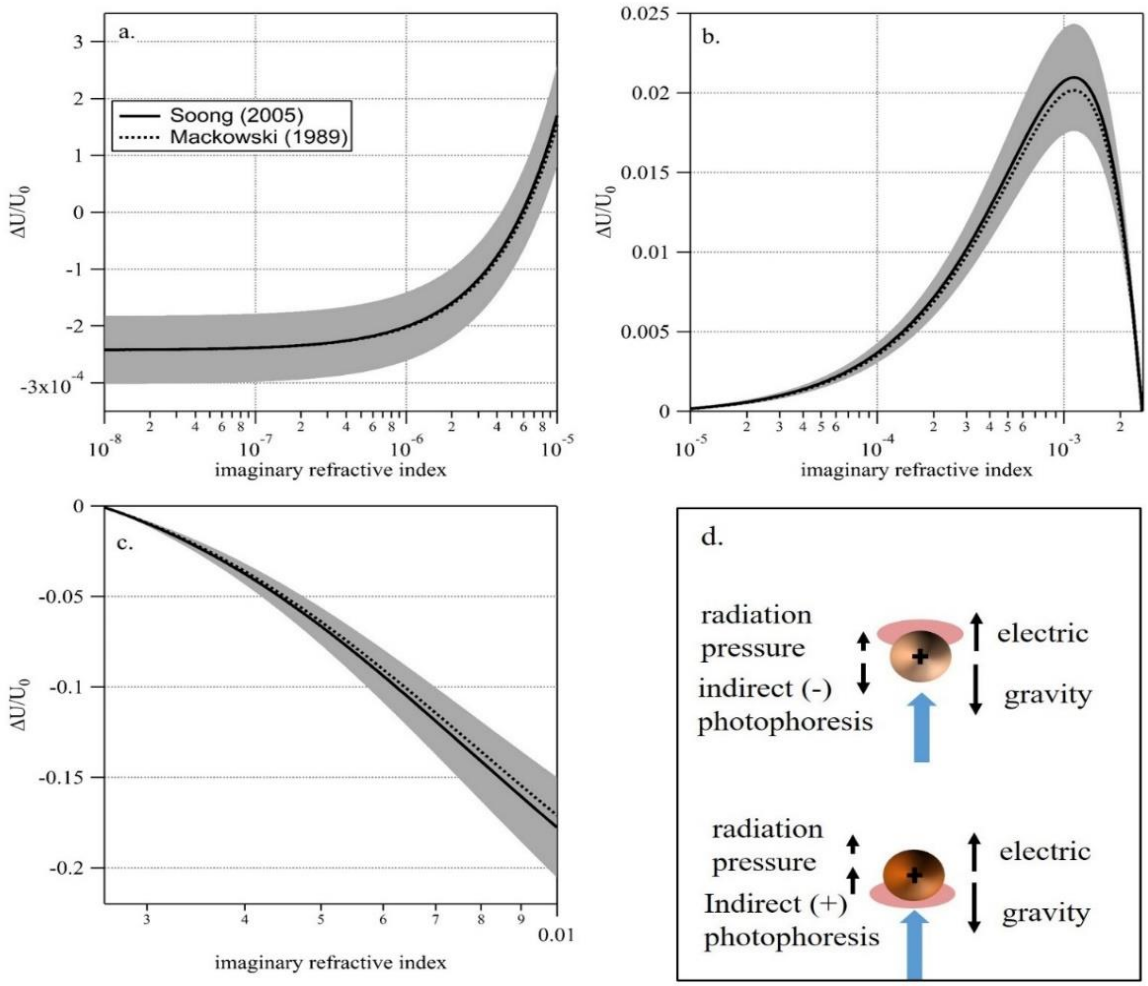

Descriptive text was added to the conclusion section in the revised version of this manuscript to describe the figure and the simulated system behavior in different absorptivity regimes.

2. Would this method be equally applicable to molecules that absorb less strongly but that are present at higher concentration?

The retrieved refractive index or the imaginary part of the refractive index, like in other retrieval methods, is that which best represent the optical properties of the measured particle. For a single composite particle that would be the refractive index of the bulk material. For a multi

component particle (miscible liquids, solutions etc.) the retrieved refractive index sometimes referred to as an effective refractive index could be different from that of the individual materials. In the results given in this manuscript, the retrieved imaginary part is not that of carminic acid and not that of PEG400. It is the imaginary part of the specific mixture and is a product of the amount of light absorbed by the particle. A different type of absorbing molecules i.e. with higher or lower molar absorptivity at higher or lower concentration would yield a different imaginary part based on the amount of light absorbed by the mixture. In this respect, this method is not different from any other retrieval method in bulk, thin film or in particle phase.

3. What range of samples/conditions (particularly RH) can this method be applied to? I would assume that any water vapor in equilibrium with the droplet would be affected by light-absorption and thus add additional complexity to the interpretation of the droplet movement with the laser illumination.

Illuminating light absorbing particle results in inevitable temperature change that is related to the amount of light absorbed and to the materials heat capacity. For the particles in this study, the temperature change is estimated to be below 1 K with using the heat conductivity equation (from 0.02 to 0.4 K, depending on κ and on the size of the particle). In equilibrium, this would also depend on the heat conductivity of the particle and its surrounding, and the surrounding temperature. A hydrated particle, upon increasing temperature, will lose some water and will reach new equilibrium with its environment at lower water activity even though the RH remains unchanged. This also means that at equilibrium the particle will be smaller. The extant of this effect depends of the temperature change within the particle. This effect was used as a method to retrieve κ (Knox & Reid, 2008; Willoughby et al., 2017). There is no theoretical limitation for retrieval of κ using EDB-PPS at elevated RH conditions. Temperature equilibrium is reached within milliseconds while water activity and size equilibrium is reached depending on the particles diffusivity. In the case of PEG400 this happens within a time scale of about 1 second. As long as equilibrium is reached, the signal can be used. The added complexity compared to a dry experiment is that parameters such as thermal conductivity of the particle and of the environment as well as the size of the particle (before and during illumination) are needed. We have performed several experiment with the PEG400-CA system at elevated RH. In these experiments, the size of the particle before illumination is retrieved with the high resolution scattering spectra as described in the manuscript, while the instantaneous size change due to water lose/gain was monitored with using low resolution scattering spectra at 1 Hz at resolution of about 1 nm (Steimer et al., 2015). It was clear that size (and water activity) equilibrium was reached within 1 second/spectrum. Further exploring this application was beyond the scope of this manuscript but will most likely be a part of future implementation of the EDB-PPS.

4. Does this measurement require the sample be dissolved in a solution with PEG400 (or similar) as a solvent? How could this technique be expanded outside of this solvent system given the need for well-characterized thermal accommodation coefficients and thermal conductivity?

This technique does not require the sample to be dissolved in PEG400 or any other solvent. The goal of this work is to retrieve low levels of κ; in a range, other particle phase techniques are

not sensitive enough. For this reason, PEG400 was used as a non-absorbing organic matrix that allows for the total absorptivity of the particle to be much lower compared to pure carminic acid. Nevertheless, as the reviewer pointed out, a disadvantage of this method is the need for some parameters to be well characterized. Amongst others these include thermal conductivity (of both particle and gas phase) and thermal accommodation coefficient.

Thermal conductivity: uncertainty in thermal conductivity leads to uncertainty in the retrieved κ. As an example, uncertainty of 30% in the thermal conductivity leads to a non-symmetric 20 – 30% uncertainty in retrieved κ in the range of 10^{-5} – 10^{-3}. The range of uncertainty is due to non-linearity of κ with $\Delta U/U_0$.

One way to reduce the uncertainty is to perform measurements of an unknown absorbing material which is highly diluted or well mixed with a well characterized material (such as PEG400, water, sulfuric acid). In this way, the thermal properties of the particle are assumed identical to the thermal properties of the well-characterized material.

An additional approach for unknown, atmospherically relevant organic material is to consider that many organic compounds are very similar with respect to their thermal properties and use an approximated value with an appropriate uncertainty. We refer the reviewer to the literature survey by Latini et al (2014) that compiled thermal conductivity data for the following 3400 data sets (excluding additional 1340 data sets of refrigerant compounds) at atmospheric pressure and reduced temperature of about 0.6 ± 0.14:

	N	**mean**	**SD**	**%SD**
Alcohols	775	0.1482	0.0256	17.3
Alkanes	1025	0.1259	0.0182	14.5
Alkenes	135	0.1301	0.0244	18.7
Aromatics	570	0.1174	0.0180	15.3
Carboxylic acids	318	0.1576	0.0427	27.1
Cycloalkanes	35	0.1262	0.0134	10.6
Cycloalkenes	10	0.1303	0.0104	8.0
Esters	236	0.1261	0.0179	14.2
Ethers	111	0.1268	0.0181	14.3
Ketones	185	0.1417	0.0203	14.3

Thermal accommodation coefficient (α_T): the literature on measurements or estimations of α_T is scarce. As a result, one must simply assume a reasonable value. It is important to note that an error in α_T propagate to relatively small errors in the retrieved κ. For example, the value that we used in this study i.e. $\alpha_T = 0.85 \pm 0.15$ ($\pm$~18%) leads to a non-symmetric 5 – 7% uncertainty in retrieved κ in the range of 10^{-5} – 10^{-3}.

This discussion was added to the last paragraph in section 3 of the revised manuscript.

5. How does ΔU/U_0 vary with a non-absorbing sample (pure PEG400 for example)? This is a necessary benchmark to show that there is no measurable effect when no absorption occurs.

For non-absorbing particle, the only effect from illuminating it would be that of the direct photophoresis (radiation pressure), which is about 1 – 2 orders of magnitude smaller than

indirect photophoresis in our experimental range. Its direction is always away from the light source so if detectable, it should result in a negative signal (i.e. negative $\Delta U/U_0$).

An experiment with undyed PEG400 particle showed no detectable signal (i.e. above noise level).

The following text was added to section 3: "It is important to note that as expected, for a pure PEG400 particle (i.e. no measurable absorption at 473 nm) at similar conditions, but a slightly less sensitive setup, no signal could be detected."

6. The main reason to make measurements on levitated droplets rather than bulk samples is that the super-saturated and super-cooled states accessible to aerosol in the atmosphere can be reproduced in a well-controlled lab environment. I would like the authors expand on the applicability of their method to these kinds of samples.

We agree with the reviewer, and mentioned in the text, that a significant disadvantage of bulk and film type of experiments is that super saturated conditions are not accessible.

This point was made clearer at the end of the introduction section of the revised version of the manuscript.

7. What causes the oscillation in the Mie resonance spectra compared to the simulation? Is this from the laser or related to the movement of the droplet with the heating beam?

If the reviewer is referring to figure 4 (previously figure 3), this figure shows the resonance peaks which are labeled on the theoretical curves and additional noise oscillations that extend the full spectra in both polarizations. These oscillations are caused mainly from variations in the laser power as the length of its optical cavity is changing. The particle horizontal movement due to the AC field sometimes causes an additional noise component. Most (but not all) of the first component is reduced by dividing the particle spectrum by a reference spectrum. Note that in this study, the particle was not illuminated with the "heating" beam while scanned with the TDL laser.

The following text was added to the figure caption: "Residual noise in the measured spectrum originate mostly from laser power oscillations due to frequency scanning operation and from horizontal oscillation of the particle due to the applied AC field."

8. Please show a figure (or SI figure) of the DC voltage as a function of time as the heating laser cycles on/off.

The following figure was added as figure 2 in the revised manuscript.

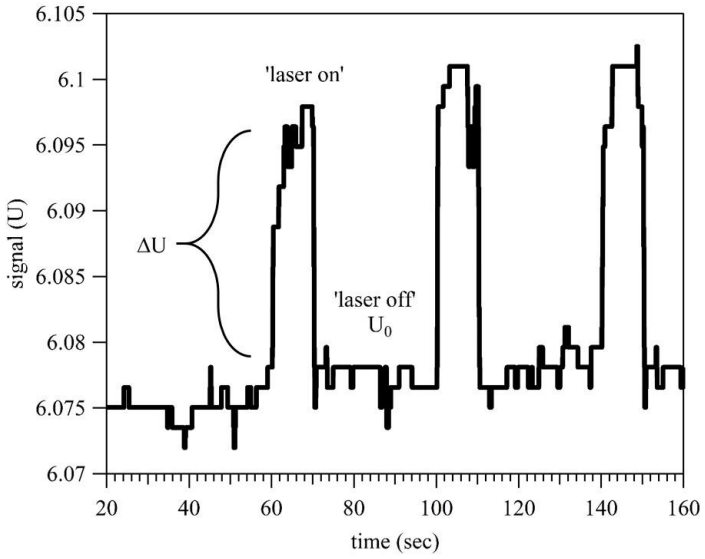

Anonymous Referee #2

Questions:
This seems to be only applicable to droplets that are neither strongly nor weakly absorbing (i.e. the *k* range of 10^{-4} to to 10^{-5} stated in the abstract).

a. Is that the actual dynamic range?

Please refer to the answer given to question #1 from referee #1. Figure 7 in the revised version was added to address this question.

b. Isn't *k* for brown carbon (BrC) typically much larger than those values? I mention this because BrC is presented as the motivation for the development of the technique.

Values of κ for BrC reported in the literature are limited by the detection limit and sensitivity of the measurement technique that is used. Therefore, a more accurate statement would be that quantifiable values of κ for BrC are typically much larger than 10^{-4} while the reality is that there is no physical lower limit for absorptivity of BrC in the atmosphere.

An alternative argument could be made that lower values of κ for aerosols are insignificant due to their low thermal effect (at least in the troposphere). It is, therefore, worth clarifying that the main motivation for the application of this technique is to measure these previously unquantifiable values and to follow evolution processes of BrC during atmospheric aging. This could mean either 'bleaching' or 'browning' and for that reason one should be able to retrieve κ at lower values that are commonly reported.

To answer this comment and comment number 6 from reviewer 1 we add the following text at the end of the introduction in the revised version of the manuscript: "With this approach we gain from combining the advantage of light absorption sensitivity nearing that of bulk UV-vis measurements with the advantage of studying chemical processes of the particle phase (accessible super saturated conditions) in an environmental chamber able to simulate a wide

range of atmospheric conditions. This could contribute to the study of light absorption evolution during atmospheric aging of BrC aerosols."

c. What atmospheric systems could this technique be applied to? I would imagine weak absorbers (e.g. aqueous sea salt aerosol) have a *k* that is too small while strong absorbers (the aforementioned BrC) have a *k* that is too large.

As mentioned above, any color forming or degrading aging processes could be relevant candidates. Oligomerization, nitrification, acid catalyzed dehydration have been reported as possible mechanism for chromophore formation. Oxidation and photooxidation reactions are known bleaching processes. One particular system of interest is browning of sulfuric acid aerosols in the presence of ketones or aldehydes. For this system, formation of UV-Vis chromophores was reported so far only in bulk and film experiment but not for aerosols.

d. Why no measurements of, for example, aqueous humic acid?

We appreciate the reviewer suggestion and agree that such a measurement would be beneficial to demonstrate the usefulness of this method. To produce a sample of humic or fulvic acid material with low absorptivity in the range of $\kappa \leq 10^{-3}$ at 473 nm it would need to be highly diluted or mixed with a non-absorbing material. This cannot be achieved with water because these particles are not sufficiently hygroscopic (additionally, we refer the reviewer to a short discussion about measurements at high RH in the answer to question 3 by reviewer #1). Unfortunately, this was attempted but could also not be achieved with PEG400 due to extremely low solubility. An additional option would be to simply use a longer wavelength for the excitation light source. This was, however, not available at the time of performing these experiments.

Minor comments:

-no need to use a non-standard symbol like χ for the size parameter when the standard *x* will do fine.

The notation for size parameter was changed from "χ" to "*x*" in the text as well as in all of the equations.

-Line 134: "retrieved by minimizing the difference between measured and calculated wavelength" I assume you mean minimizing the sum of squared differences?

What was actually done was to minimize the sum of the absolute value of the differences. This was added in the text.

-use of the times symbol in many equations is unnecessary.

To improve clarity, the multiplication symbol was removed from all equations.

-Line 225: What is the viscosity of PEG400?

A range of viscosity values for PEG400 as reported by the supplier (Merck), at 293.15 K was added to the text; 105 - 130 mPa sec.

-Line 269: "473-nm" to "473 nm"

This was correct in the text.

-Figure 2 caption: intensity units are italics when they should not be

This was corrected in the text.

Additional changes in the revised version of the manuscript:

1) In figure 5 (previously figure 4), the units of the X axis were changed from mbar to hPa to match the units used in the text.
2) The Y axis of figure 6 (previously figure 5) was changed to log scale.
3) Several typos were identified and corrected.

Knox, K. J., & Reid, J. P. (2008). Ultrasensitive absorption spectroscopy of optically-trapped aerosol droplets. *Journal of Physical Chemistry A*, *112*(42), 10439–10441. https://doi.org/10.1021/jp807418g

Latini, G., Di Nicola, G., & Pierantozzi, M. (2014). A critical survey of thermal conductivity literature data for organic compounds at atmospheric pressure and an equation for aromatic compounds. *Energy Procedia*, *45*, 616–625. https://doi.org/10.1016/j.egypro.2014.01.066

Steimer, S. S., Krieger, U. K., Te, Y. F., Lienhard, D. M., Huisman, A. J., Luo, B. P., Ammann, M., & Peter, T. (2015). Electrodynamic balance measurements of thermodynamic, kinetic, and optical aerosol properties inaccessible to bulk methods. *Atmos. Meas. Tech.*, *8*(6), 2397–2408. https://doi.org/10.5194/amt-8-2397-2015

Willoughby, R. E., Cotterell, M. I., Lin, H., Orr-Ewing, A. J., & Reid, J. P. (2017). Measurements of the Imaginary Component of the Refractive Index of Weakly Absorbing Single Aerosol Particles. *Journal of Physical Chemistry A*, *121*(30), 5700–5710. https://doi.org/10.1021/acs.jpca.7b05418

Photophoretic spectroscopy in atmospheric chemistry – high sensitivity measurements of light absorption by a single particle

Nir Bluvshtein, Ulrich K. Krieger, Thomas Peter

Institute for Atmospheric and Climate Science, ETH Zurich, 8092, Switzerland

Correspondence to: Nir Bluvshtein (nir.bluvshtein@env.ethz.ch)

Abstract. Light absorbing organic atmospheric particles, termed brown carbon, undergo chemical and photochemical aging processes during their lifetime in the atmosphere. The role these particles play in the global radiative balance and in the climate system is still uncertain. To better quantify their radiative forcing due to aerosol-radiation interactions, we need to improve process level understanding of aging processes, which lead to either 'browning' or 'bleaching' of organic aerosols. Currently available laboratory techniques aim to simulate atmospheric aerosol aging and measure the evolving light absorption, but suffer from low sensitivity and precision. This study describes the use of electrodynamic balance photophoretic spectroscopy (EDB-PPS) for high sensitivity and high precision measurements of light absorption by a single particle. We demonstrate the retrieval of time-evolving imaginary part of the refractive index for a single levitated particle in the range of 10^{-4} to 10^{-5} with uncertainties of less than 25% and 60%, respectively. The experimental system is housed within an environmental chamber, in which aging processes can be simulated in realistic atmospheric conditions and lifetime of days to weeks. This high level of sensitivity enables future studies to explore the major processes responsible for formation and degradation of brown carbon aerosols.

1 Introduction

Most radiative transfer schemes in climate models treat organic aerosol, a major subset of atmospheric aerosols that comprise 20-90% of the total particulate mass (Kanakidou et al., 2005; Zhang et al., 2007), as non-absorbing in the UV-Vis wavelength range, attributing them with a negative (cooling) radiative effect. However, light absorbing organic aerosol, termed brown carbon (BrC), with wavelength dependent light absorption ($\lambda^{-2} - \lambda^{-6}$) in the UV-Vis wavelength range (Chen and Bond, 2010; Hoffer et al., 2004; Kaskaoutis et al., 2007; Kirchstetter et al., 2004; Lack et al., 2012b; Moosmuller et al., 2011; Sun et al., 2007), may be the dominant light absorber downwind of urban and industrialized areas and in biomass burning plumes (Feng et al., 2013). Recently, it has been shown that including BrC absorption properties in radiative transfer models lead to a stronger wavelength dependency of light absorption by aerosols and to significant changes in the overall effective radiative

forcing from aerosol-radiation interactions (ERFari) (Feng et al., 2013; Lack and Cappa, 2010). Atmospheric aging processes of organic aerosol can lead, through complex mechanisms, to formation of light absorbing compounds ('browning') or to their degradation ('bleaching'). The accurate characterization of these processes is one of the main open questions in atmospheric chemistry research and has been the focus of many recent studies (see Laskin et al. (2015) for a review). Although significant advances have been made, the contribution of BrC to anthropogenic radiative forcing still poses significant uncertainty. The estimated ERFari attributed to BrC is 0.1 to 0.25 W m^{-2}, offsetting 10 to 25% of the global mean aerosol cooling effect ($-1.1^{-0.1}_{-1.95}$ W m^{-2}) (Bond et al., 2013; Brown et al., 2018; Feng et al., 2013; Myhre et al., 2013). On a regional scale surrounding mega-cities and industrial areas, this value may be up to an order of magnitude higher (Feng et al., 2013), which nearly doubles the local warming effect caused by the increase in the CO_2 concentration. For this reason, it is imperative to (i) better understand the formation and degradation of BrC aerosols resulting from chemical and photochemical aging processes (Dasari et al., 2019; Drozd and McNeill, 2014; Hems and Abbatt, 2018; Lambe et al., 2013; Lee et al., 2013, 2014; Marrero-Ortiz et al., 2019; Powelson et al., 2014; Romonosky et al., 2015; Saleh et al., 2014; Schnitzler and Abbatt, 2018; Zhao et al., 2015; Zheng et al., 2013), (ii) quantify the BrC wavelength dependent light absorption and (iii) identify the main molecular species responsible for this absorption.

Laboratory studies simulating BrC formation and degradation mechanisms generally take one of two approaches to quantify wavelength dependent light absorption in the UV-Vis wavelength range, which is described using the imaginary part (κ) of the complex refractive index (CRI; $m = n + i\kappa$). The first approach uses bulk liquid phase or gas–liquid multiphase experiments to simulate atmospheric chemical processes. This is then followed by UV-Vis spectroscopy absorption measurements (Nguyen et al., 2012; Nozière et al., 2010; Nozière and Córdova, 2008; Updyke et al., 2012). The advantages are high sample volume available for analysis, and the extremely high sensitivity of UV-Vis absorption spectroscopy. The disadvantage is that supersaturated conditions often encountered in atmospheric aerosol particles are impossible to generate in a bulk volume. This is an important disadvantage of the bulk approach as chemical activity, viscosity and diffusivity under supersaturated conditions may alter the chemical aging significantly.

The second approach uses an environmental chamber, reactor, or flow tube to reproduce atmospheric processes. In this context, particles are generated by aerosolization into the experimental volume or by gas phase chemistry leading to reduced volatility of precursor compounds with subsequent gas-to-particle conversion. These aerosols are then subjected to chemical or physical aging processes using radiation, relative humidity and reactive gaseous components. The aged material may then be collected on filter substrates, extracted with a liquid solvent and analyzed by UV-Vis spectroscopy. Alternatively, aerosols may be measured with a suite of particle-ensemble, flow-through optical methods, such as cavity enhanced and photoacoustic spectroscopy, for both direct and indirect measurements of light absorption (Flores et al., 2014a, 2014b; He et al., 2018; Nakayama et al., 2013). To maintain particle size and concentration high enough for analysis using these techniques and to simulate atmospheric exposure of up to several days, precursor concentrations often far exceed those of the ambient atmosphere. This difference in environment between the reactor and the real atmosphere may affect the final distribution of products after multi-generation chemical aging, which may lead to misleading interpretations of the experimental results. An

advantage of the optical instruments compared with the filter extraction techniques is the independence from solubility, extraction efficiency and solvent matrix effects. Additionally, particles are measured *in-situ* and with higher time resolution. Disadvantages are the relatively low sensitivity to absorption and, for some instruments, the frequent need for calibration (Lack et al., 2012a). As a result, κ for BrC aerosols is often reported with values near the limit of quantification of the retrieval technique, or that actually conflicts with results from analyses of similar chemical systems (Liu et al., 2013, 2012; Nakayama et al., 2013; Ofner et al., 2011) and with uncertainties that can exceed 100% (Bluvshtein et al., 2016; Flores et al., 2014a, 2014b; He et al., 2018; Lack et al., 2012b; Lavi et al., 2013; Nakayama et al., 2010, 2013; Trainic et al., 2011; Washenfelder et al., 2013).

To make significant progress, reduce uncertainties, and resolve contradictions, this study aims to extend the approach of electrodynamic balance photophoretic spectroscopy (EDB-PPS) for high sensitivity and high precision measurements of UV-Vis light absorption by a single particle, in an environmental chamber, exposed to realistic atmospheric aging processes.

Photophoresis describes the optical forces acting on an illuminated particle. Direct photophoresis (or "radiation pressure" force; F_{rp}), always in the direction of light propagation (away from the light source) and indirect photophoresis (F_{ph}), a less recognized force, central to this work, that strongly depends on the absorption of light. Unlike radiation pressure, indirect photophoresis is a result of an uneven temperature distribution on the surface of the particle resulting from absorption. It acts through momentum transfer with the surrounding gas molecules, and thereby it is temperature and pressure dependent. To resolve the direction (away from or towards the light source) and the magnitude of the indirect photophoresis force one needs to determine the internal electric field distribution (Bohren, 1983; Mackowski, 1989). Pope et al. (Pope et al., 1979) and Arnold et al. (Arnold et al., 1980) conceived the idea of PPS on a single levitated particle and described the spectrally dependent ratio of the measured photophoretic force to the gravitational force on the particle. Building upon their seminal work with following developments in the mathematical description of indirect photophoresis (Beresnev et al., 1992; Mackowski, 1989; Rohatschek, 1995), computational advances in Mie theory and internal field calculation (Hovenier, 2000), we extend the use of PPS. Here we describe how PPS can be used for high sensitivity retrieval of the imaginary part of the refractive index of organic aerosol proxy particles levitated in an environmental chamber EDB and subject to aging processes. The EDB is a well-established tool in atmospheric science, used for the study of thermodynamic and chemical properties of single levitated particles (Krieger et al., 2000; Steimer et al., 2015; Tang and Munkelwitz, 1994; Zardini et al., 2008). Its high sensitivity to changes in the net vertical force acting on the particle makes it ideal for measurements of photophoresis, i.e. the miniscule optical forces acting on the levitated particle as a result of its interaction with light. With this approach we gain from combining the advantage of light absorption sensitivity nearing that of bulk UV-Vis measurements with the advantage of studying chemical processes in the particle phase (accessible super saturated conditions) in an environmental chamber able to simulate a wide range of atmospheric conditions. This could contribute to the study of light absorption evolution during atmospheric aging of BrC aerosols.

Deleted: v

2 Experimental

2.1 Electrodynamic balance

Over 100 years ago Robert Millikan and Harvey Fletcher, in their famous oil drops experiment, showed that tuning the electric potential between two capacitor plates, required to levitate a charged particle, can be used as a balance with a sensitivity of about 10^{-13} g. Today, the electrodynamic balance (EDB) is an established tool used to derive thermodynamic and physical information of a single, levitated particle. The EDB used in this study (Figure 1) is based on the double-ring design characterized by Davis et al. (Davis et al., 1990) and described in previous publications (Colberg et al., 2004; Steimer et al., 2015). Only a brief description follows. The EDB is hosted within a 180 cm^3 environmental chamber, which allows temperature and pressure regulation with precision of ±0.02 K and ±2 hPa. Mass flow controllers are used to regulate gas flow rate and composition to 5 ccm of dry N_2. A single-droplet generator (Hewlett-Packard 51633A ink jet cartridge) is used to inject an electrically charged diluted aqueous solution of the sample material to the center of the trap. After complete loss of water, the resulting particle (typically 7-13 µm in radius) is balanced by a DC voltage that is regulated with a 25 Hz automated video feedback loop. The DC voltage (U) that is applied between the EDB endcap electrodes, to hold the particle in the center of the trap, is proportional to the net vertical force acting on the particle. A sensitivity on the applied DC voltage as low as 0.01% is equivalent to changes in mass in the range of 10^{-13} to 10^{-12} g depending on the particle's size and density. This is commonly used to measure small changes in particle mass due to loss or uptake of gaseous components by the particle (Steimer et al., 2015; Tang and Munkelwitz, 1994; Zardini et al., 2008). In this study, we alternately illuminate a suspended particle with a 473 nm, 33 mW mm^{-2} (±15%) diode laser (Laser Quantum, gem 473) at 25% duty 40 sec cycles (Figure 1b). Variations in the DC voltage from 'laser off' to 'laser on' (Figure 2, $\Delta U/U_0$) in each cycle were used to measure changes in the net vertical force induced by illumination of the particle:

$$\frac{\Delta U}{U_0} = \frac{U_{on} - U_{off}}{U_{off}} = \frac{F_{ph} + F_{rp}}{F_g + F_s} . \quad (1)$$

Here, F_{ph} and F_{rp} are the indirect photophoretic and radiation pressure forces. The subscripts "on" and "off" relate to the light source. Gravity (F_g) and Stokes drag (F_s) caused by the gas flow, are constant at the time scale of the measurement, and are given by

$$F_g = \frac{4}{3}\pi a^3 \rho_p g , \quad (2)$$

$$F_s = \frac{6\pi a \eta q_v}{C_c S} , \quad (3)$$

where a and ρ_p are radius and mass density of the levitated particle, g is the standard acceleration due to gravity, η is the gas dynamic viscosity, q_v is volumetric flow rate, S is a characteristic flow cross section and C_c is the Cunningham slip correction factor (Kim et al., 2005). This formulation enables the direct measurement of the sum of the optical forces ($F_{ph} + F_{rp}$), which are related to the particle size and CRI. After determining the particle size and the real part of the refractive index n (Section 2.2.), the sum $F_{ph} + F_{rp}$ is iteratively calculated by varying κ to minimize the difference between the measured and calculated $\Delta U/U_0$.

Deleted: ,
Deleted: with sensitivity
Deleted: , which
Deleted: a
Deleted: ofabout
Deleted: 5
Deleted: -

The following section describes how the particle size and real refractive index are determined from high-resolution light scattering measurements and Section 2.3 describes how F_{ph}+F_{rp} is finally calculated and used to retrieve the imaginary part of the CRI.

2.2 Determination of size and real refractive index

Mie resonance spectroscopy is used to simultaneously retrieve the particle's radius (a) and real part (n) of the CRI defined as:

$$a = \frac{\lambda x}{2\pi}\,, \tag{4}$$

and

$$n(\lambda) = n_D + m_1\left(\frac{1}{\lambda^2} - \frac{1}{\lambda_D^2}\right). \tag{5}$$

Here, $n(\lambda)$ is the wavelength-dependent real refractive index, n_D is the refractive index at the sodium D-Line, m_1 is a dispersion coefficient and x is the size parameter. Polynomial regression parameters between the refractive index and size parameter of transverse electric (TE) and transverse magnetic (TM) mode resonances were calculated (Lam et al., 1992; Preston and Reid, 2013, 2015) and a look-up table of these parameters was generated for all possible TE and TM resonances with order numbers of 3 to 8 and mode numbers of 26 to 180. We obtained high-resolution spectra by illuminating the levitated particle with a tunable diode laser at both parallel and perpendicular linear polarizations (TDL, New Focus, model Velocity 6312) in the range λ = 765–781 nm and recording the elastic light scattering at $\pi/2$ angle (Steimer et al., 2015) (Figure 1a,4). Then, a, n_D and m_1 are retrieved by minimizing the sum of absolute values of the differences between measured and calculated wavelengths of the Mie resonances over the three dimensional parameter space.

2.3 Photophoretic spectroscopy

Direct photophoresis or radiation pressure is readily calculated from

$$F_{\mathrm{rp}} = (Q_{\mathrm{ext}} - Q_{\mathrm{bs}})\frac{\pi a^2 I}{c}, \tag{6}$$

where I is the radiant flux density (in W/m^2) and c is the speed of light. Q_{ext} and Q_{bs} are Mie extinction and back scattering efficiencies (unitless). We use the Mie MatLab functions developed by Mätzler (2002) to calculate the efficiencies.

Indirect photophoresis (F_{ph}) is directed away from the light source for a highly absorbing particle (positive photophoresis) but towards the light source for low absorptivity (negative photophoresis). This is a result of the structure of the internal electric field within a spherical particle interacting with radiation. Multiple refractions and internal reflections lead to size dependent, nano-focusing of the incident beam within the particle volume. For particles larger than the wavelength of the incident light, the energy is "focused" closer to the non-illuminated side of the particle. In highly absorbing particles, however, most of the energy is absorbed by the illuminated hemisphere of the particle, heating it more than the "dark" hemisphere. Therefore, a key parameter determining the direction and amplitude of F_{ph} is the temperature asymmetry parameter (J), resulting from the

Deleted: ×

Formatted: Font: Italic

Deleted: χ

Deleted: 3

Deleted: ×

Deleted: Matlab

uneven internal electric field and, consequently, uneven temperature distribution (Yalamov et al., 1976). To calculate J, one can use an integration of the source function over the particle volume:

$$J(\chi, m) = 3n\kappa\chi \int_0^1 \int_{-1}^1 B(t,\mu) t^3 \mu d\mu \, dt \, . \quad (7)$$

Here $B(t,\mu)$ is the dimensionless electric field distribution inside the particle, t (fraction of a) and $\mu = \cos\theta$ are the spherical coordinates. Simply put, J indirectly describes the temperature gradient between the illuminated and the "dark" side of the particle surface.

Unlike radiation pressure, F_{ph} acts through the presence of gas molecules around the illuminated particle. Impaction and reflection of the surrounding gas molecules, and consequent momentum transfer with the particle's surface, is temperature dependent and thus leads to a net force directed from the warmer to the colder particle hemisphere. Indirect photophoresis is also strongly pressure (p) dependent. It reaches its maximum value at pressures, where the Knudsen number (Kn = L/a) is around unity, i.e. where the gas mean free path (L) is comparable to the radius of the particle (a). In the free molecular regime, i.e. Kn >> 1, F_{ph} is proportional to p, whereas in the continuum regime, i.e. Kn << 1, F_{ph} is inversely proportional to p. Rohatschek (1995) provided a pressure dependent model of F_{ph} interpolating previous formulations at the two pressure regime limits. His approach provides a convenient estimate of F_{ph} between the free molecular and continuum limits:

$$F_{ph} = \frac{2F_{max}}{p/p_{max} + p_{max}/p} \, , \quad (8)$$

with

$$F_{max} = D \frac{a^2 JI}{k_p} \sqrt{\frac{\alpha_T}{2}} \, , \quad (9)$$

$$p_{max} = D \frac{3T}{\pi a} \sqrt{\frac{2}{\alpha_T}} \, , \quad (10)$$

where α_T is the thermal accommodation coefficient, k_p is the particle thermal conductivity and T is the gas temperature away from the particle surface. Further, D relates to gas phase parameters as follows:

$$D = \frac{\pi \hat{c} \eta}{2T} \sqrt{\frac{\pi C_s}{3}} \, , \quad (11)$$

where C_s is the thermal slip coefficient and $\hat{c}$ is the mean thermal velocity of the gas molecules

$$\hat{c} = \sqrt{\frac{8RT}{\pi M}} \, , \quad (12)$$

in which R is the gas constant and M is the gas molar mass.

Our experimental set up (particle radius of 7-13 µm and pressure range of 400-800 hPa) is limited to Kn = 0.0075-0.03. We are therefore constrained to a transition flow regime referred to as the slip-flow regime (typically 10^{-2} < Kn < 10^{-1}), where F_{ph} deviates significantly from Rohatschek's interpolation. Mackowski (1989) presented an analytical solutions of the spherical geometry heat conduction equation in three dimensions for calculating F_{ph} in the slip-flow regime by adding a tangential velocity slip boundary condition (also referred to as thermal stress slip flow) to the continuum regime solution of Yalamov et al. (1976):

Deleted: χ

Deleted: χ

Deleted: interpolating

Deleted: mbar

$$F_{\mathrm{ph}} = -\frac{4\pi C_s \eta^2 I a J}{\rho_g k_p T}\left[(1+3C_m\mathrm{Kn})\left(1+2C_t\mathrm{Kn}+2\frac{k_g}{k_p}\right)\right]^{-1}. \quad (13)$$

The momentum exchange coefficient is taken as $C_m = 1.175 \pm 0.175$ (Reed, 1977), while the thermal slip (C_s) (Ivchenko et al., 1993) and temperature jump (C_t) (Loyalka, 1968) coefficients

$$C_s = \frac{3}{2}\left(\frac{0.4375+0.2084\alpha_T}{0.856+0.1092\alpha_T}\right), \quad (14)$$

$$C_t = \frac{5}{18}\frac{2-\alpha_T}{\alpha_T}(1+0.1621\alpha_T), \quad (15)$$

are functions of the thermal accommodation coefficient α_T. Here we used a value of $\alpha_T = 0.85 \pm 0.15$ to accommodate a range of values published for a variety of materials (Ganta et al., 2011; Li et al., 2001; Shaw and Lamb, 1999; Trott et al., 2007). It was shown that with increased absorption (i.e. steep interface temperature jump) or decreasing particle size, Equation (14) deviates from experimental measurements (Mackowski, 1989; Soong et al., 2010). A solution to this problem was presented by Soong et al. (2010) who adopted a modified slip boundary condition from Lockerby et al. (2004). The authors developed the following correction to Mackowski's solution:

$$F_{\mathrm{ph\_corr}} = F_{\mathrm{ph}}\left(1+\frac{2C_m\mathrm{Kn}}{C_s}\right). \quad (16)$$

From equation (16) it is clear that at $\mathrm{Kn} \ll 1$ the correction factor approaches unity. For the purpose of this study, i.e. low absorptivity particles and Kn = 0.0075-0.03, the correction is small, but we nevertheless apply it in our evaluation and term the corrected photophoretic force hereafter F_{ph}.

As mentioned above, J is the key parameter linking the particle's CRI to F_{ph}. Mackowski (1989) also presented an expression for J by analytical integration of equation (7):

$$J = -\frac{6n\kappa}{|m|^2 x^3}\mathrm{Im}\sum_{N=1}^{\infty}\left(\frac{N(N+2)}{m}\left(\frac{c_{N+1}c_N^* R_N}{C_N}+d_{N+1}d_N^* R_{N+1}C_N^*\right)-\left(\frac{N(N+2)}{N+1}\left(\frac{c_{N+1}c_N^*}{C_N}+\frac{d_N d_{N+1}^*}{C_N^*}\right)+\frac{2N+1}{N(N+1)}d_N c_N^*\right)S_N\right), \quad (17)$$

where the coefficients C_N, R_N and S_N are

$$C_N = \frac{N+1}{m\chi}-\frac{\psi_N'(m\chi)}{\psi_N(m\chi)}, \quad (18)$$

$$R_N = \frac{\mathrm{Im}(mC_N)}{\mathrm{Im}(m^2)}, \quad (19)$$

$$S_N = \frac{i}{2\mathrm{Im}(m^2)}\left\{\chi(m+m^*|C_N|^2)-\left(m+2(N+1)\frac{\mathrm{Re}(m^2)}{m}\right)R_N+(2N+1)m^*|C_N|^2 R_{N+1}\right\}, \quad (20)$$

$$c_N = \psi_N(m\chi)\tilde{c}_N, \quad (21)$$

$$d_N = \psi_N(m\chi)\tilde{d}_N. \quad (22)$$

Here, $\tilde{c}_N$ and $\tilde{d}_N$ are the Mie coefficients for the internal field, computed using the MatLab Mie routines by Mätzler (2002) and Ψ_N is the Ricatti-Bessel function of order N. For clarity, the prime denotes the differentiation with respect to the argument in brackets and the superscript * denotes the complex conjugate. Figure 3 shows F_{ph} calculated with the above three models over a wide pressure range extending from the free molecular to the continuum flow regimes. From eq. (13) and Figure 3, one

Deleted: ×
Deleted: ×
Deleted: ×
Deleted: ×
Deleted: ×
Deleted: χ
Deleted: ×
Deleted: χ
Deleted: 2
Deleted: 2

can show that Mackowski's formulation equals Rohatschek's solution at the continuum limit (i.e. Kn $\ll 1$) only for particles that are good heat conductors compared with the surrounding gas (i.e. $k_g/k_p \ll 1$).

For applications involving slightly absorbing ($\kappa \leq 10^{-3}$) micron-sized, organic particles, the indirect photophoretic force is generally 1-2 orders of magnitude larger than radiation pressure but about 2-3 orders of magnitude lower than gravity. High sensitivity and stability of the EDB is therefore imperative for high sensitivity retrieval of κ from EDB-PPS measurement.

3 Results and discussion

To test the methodology a slightly absorbing organic particle with known CRI and thermal properties is required. For this purpose, we selected PEG400 (polyethylene glycol with mean molecular weight of ≈ 400 g mol^{-1}) as a proxy. PEG400 has the advantage of being an organic, non-volatile liquid, miscible with water (needed for injection of a droplet into the EDB). Additionally, PEG400 has well characterized optical and thermodynamic properties (Francesconi et al., 2007; Han et al., 2008; Marcos et al., 2018; Reyes et al., 2000), which we assume to be unchanged by addition of 0.23% wt (0.19% mole) of carminic acid (CA, Sigma-Aldrich). The imaginary part of the refractive index for this PEG400-CA solution ($\kappa = (1.394 \pm 0.05) \times 10^{-4}$) was determined with a simple Beer-Lambert setup composed of the 473 nm laser introduced in Section 2.1, a 1 mm cuvette, a power meter and using the following relations (Sun et al., 2007):

$$A = \log_{10}\frac{I_0}{I} = \alpha L\,, \quad (23)$$

$$\alpha = \frac{4\pi\kappa}{\lambda}\,, \quad (24)$$

where A is the optical attenuation or absorption of a bulk sample with an optical path length L and attenuation coefficient α at wavelength λ. Combining equations (23) and (24) leads to:

$$\kappa = \frac{A\ln(10)\lambda}{4\pi L}\,. \quad (25)$$

High viscosity of the PEG400 (105 - 130 mPa sec at 293 K; Merck) leads to slight heterogeneity of the liquid in the cuvette. For this reason, we repeated this spectroscopic measurements with the laser beam (< 1 mm in diameter) crossing the cuvette at different positions on its surface. This led to the 3.6% uncertainty in the value of κ stated above.

A droplet with 3% wt of the PEG400-CA solution in water was injected into the EDB under dry N_2 flow as described in Section 2.1. Following size stabilization and water evaporation, high-resolution Mie resonance spectra were measured to determine the particle real part of the CRI (n_D = 1.4665, m_1 = 2745) and size (a = 9.2906 μm). Figure 4 shows the measured TE and TM modes spectra and the fitted resonance peaks along with their identification by order (l) and mode (n) numbers. Figure 5 shows the response of the EDB to changes in the net vertical force due to illumination of the levitated particle ($\Delta U/U_0$) at different pressure values within the range of our experimental set up. Also shown in Figure 5 is the response calculated using the three models described in Section 2.3. It is clear that both the Mackowski and the Soong formulations, which are barely distinguishable within the resolution of Figure 5, fit the measured data very well, whereas the Rohatschek interpolation, which

Deleted: -
Deleted: ×
Deleted: ×
Deleted: ×
Deleted: ×
Deleted: ×
Deleted: 3
Deleted: 4
Deleted: 4
Deleted: 4

assumes $k_g/k_p \ll 1$ and does not account for slip-flow conditions, overestimates the response. The error bars on the measured data represent the standard deviation over five illumination cycles and the gray shaded area represents the uncertainty propagated through the Soong model calculation. The major contributor to the latter is a 15% uncertainty on the radiant flux, which is measured in our experiment with a power meter (nova-display, Ophir Optronics LTD) and a beam profiler (CMOS-1.001- Nano, CINOGY Technologies GmbH).

It is important to note that as expected, for a pure PEG400 particle (i.e. no measurable absorption at 473 nm) at similar conditions, but a slightly less sensitive setup, no signal could be detected.

To further demonstrate the potential of the EDB-PPS approach in determining the imaginary RI with high sensitivity and precision, an additional particle from the same PEG400-CA batch, with radius of 12.858 µm was levitated and the response of the EDB to change in the net vertical force was recorded over about 16 hours of illumination cycles. To take advantage of the inverse pressure dependence of the photophoretic effect, this experiment was conducted at 400 hPa, which is at the lower limit of our experimental set up. Figure 6 shows the measured $\Delta U/U_0$ and the point-by-point retrieved κ, which decreases from about 1.25×10^{-4} to about 0.06×10^{-4} over the "laser on" time (i.e. 25% of the total experiment time). Both traces demonstrate a decay feature as a result of slow photolysis of the CA (Jørgensen and Skibsted, 1991). The initial retrieved value $\kappa = (1.251^{+0.315}_{-0.213}) \times 10^{-4}$ is about 20% lower than the value retrieved from the bulk cuvette experiment [$\kappa = (1.394 \pm 0.05) \times 10^{-4}$] but with overlapping uncertainty range. The overall uncertainty in retrieved κ demonstrated in Figure 6b is estimated to be up to 25% for $\kappa \approx 10^{-4}$ and up to 60% for $\kappa \approx 10^{-5}$. The gray shaded area on the $\Delta U/U_0$ plot (Figure 6a) is the uncertainty in each $\Delta U/U_0$ data point determined from the standard deviation on the value of U averaged during "laser off" and "laser on" stages of each individual illumination cycle. These experimental uncertainties, with values of 2×10^{-5} - 10×10^{-5} (unitless) together with point-by-point variability of up to $\pm10^{-4}$, are a result of the sum of system instabilities. These are independent of the value of $\Delta U/U_0$ and are a significant component limiting the sensitivity to κ of this experimental approach. The experimental uncertainty contributes up to 10% uncertainty on the value of the retrieved κ for values down to $\kappa \approx 2 \times 10^{-5}$ and about 30% for $\kappa < 2 \times 10^{-5}$. The uncertainty on the radiant flux used in the model calculation is the major limiting factor for the sensitivity of the experimental approach contributing about 15% to the uncertainty of the retrieved κ down to $\kappa \approx 2 \times 10^{-5}$.

We determine the overall sensitivity of this approach to the imaginary RI (within the limitation of our experimental setup) to be in the range of 1×10^{-5} - 2×10^{-5}. The accumulated uncertainty of κ from all other parameters in Equations (14) and (17) is below 10% for κ down to $\kappa \approx 2 \times 10^{-5}$. These include uncertainties in the particle size, real part of the CRI, density and thermal properties. However, the major contributor to this uncertainty is the range of selected values of the thermal accommodation coefficient mentioned in section 2.3. An uncertainty of 18% on the thermal accommodation coefficient ($\alpha_T = 0.85 \pm 0.15$) propagates to 4% – 7% uncertainty on the retrieved κ. This small contribution to the overall uncertainty demonstrates the usefulness of the EDB-PPS approach for the retrieval of the imaginary RI of organic particles with unknown

Deleted: 5
Deleted: 01
Deleted: 5
Deleted: 5
Deleted: 5

composition following accurate Mie resonance spectroscopy (for determination of size and real RI) as long as assumptions of sphericity and homogeneity hold.

Additional potential source for uncertainty in case the particle is composed mostly of unknown or not well-characterized substances is the particle's thermal conductivity. A solution would be to consider that many organic compounds are very similar with respect to their thermal properties and use an approximated value with an appropriate uncertainty. Latini et al. (2014) published a literature survey of 4740 thermal conductivity data sets of organic compounds at atmospheric pressure and reduced temperature of about 0.6 ± 0.14. A partial list of the data from this publication (excluding 1340 data sets of refrigerant compounds) is presented in Table 1. The list clearly show the similarity in thermal conductivity for many organic compounds abundant in atmospheric aerosols.

4 Conclusion

This study demonstrates the usefulness of the electrodynamic balance – photophoretic spectroscopy (EDB-PPS) technique to retrieve the imaginary component of the complex refractive index of a slightly absorbing organic particle levitated in an environmental chamber. We showed agreement between measurements and model calculation and reliable retrieval of the imaginary RI at a wavelength of 473 nm, in the range of $10^{-5} \leq \kappa \leq 10^{-4}$ with uncertainty of about 25% for $\kappa = 10^{-4}$ and 60% for $\kappa = 10^{-5}$. The major limiting factor for sensitivity and precision within our setup is the uncertainty in the radiant flux.

In this study, we chose to emphasize the usefulness of EDB-PPS at the lower range of κ due to availability of other, simpler to implement, particle phase techniques suitable for retrieval of higher values of κ. Nevertheless, EDB-PPS is not limited to $10^{-5} \leq \kappa \leq 10^{-4}$. Figure 7 shows a simulated signal ($\Delta U/U_0$) over 6 orders of magnitude of κ, from 10^{-8} to 10^{-2}, for a PEG400 based particle with a radius of 10 μm, At the lower end of this range (left side of figure 7a) κ is effectivity zero and the simulated signal is negative (i.e. the particle moves away from the light source) due to direct photophoresis (radiation pressure) alone. Note how, as κ increases, the signal increases to positive values (figure 7a and 7b) due to an increase in the thermal asymmetry parameter that results in negative indirect photophoresis. With additional increase in κ, more energy is absorbed on the illuminated side of the particle. This offsets the hotspot of absorbed energy on the surface of the 'dark' side of the particle. As a result, the thermal asymmetry parameter and the magnitude of the signal are reduced. As κ continues to increase the asymmetry parameter changes sign from positive to negative as the illuminated side of the particle becomes warmer than the 'dark' side. This is shown in figure 7c as negative signal and illustrated in 7d as the particle shifts from the regime described in the upper part of figure 7d to the one described by lower part. Based on this simulation and on our system's sensitivity limitations we determined the lower limit for retrieval of κ at 10^{-5} and do not determine an upper limit. We do however, note areas with high uncertainty, namely, around $\kappa \approx 10^{-3}$, where the change in signal flattens and around the point where the regime changes from negative to positive indirect photophoresis. The latter depends heavily on the particle size. An important caveat is the non-injective behavior observed in figure 7b were two values of κ could solve for the same signal. To address the issue

one would need to have prior knowledge on the order of magnitude of the particle's absorption (for example; below or above $\kappa = 10^{-3}$). Alternatively, in aging experiments, as κ evolves, the direction of the change of the signal would clarify the direction of the change of κ.

The range of environmental conditions allowed by the chamber are pressure of 400 – 800 hPa, RH of 0 – 90% and temperature of 200 – 300 K. This means that we can measure and understand heterogeneous chemistry and photochemical aging processes of a single particle in the full range of boundary layer conditions with atmospherically relevant gas concentration and residence time. The combination of high sensitivity and quantification level with the wide application range of the environmental chamber enables us to improve process level understanding of formation and degradation of BrC aerosols resulting from chemical and photochemical aging processes that is beyond the reach of previously available aerosol flow-through techniques. This study laid the needed foundations for future development of a new methodology aimed to simultaneously measure the evolution of light absorption and the molecular composition of atmospheric aerosol proxies by coupling photophoretic spectroscopy to an electrodynamic balance – soft ionization mass spectroscopy (EDB-MS) (Birdsall et al., 2018). This will lead to a step change in our understanding of how such particles evolve in the atmosphere by directly linking optical properties to chemical composition.

Deleted: proxies of

Deleted: s

Data availability. For data related to this paper, contact Nir Bluvshtein (nir.bluvshtein@env.ethz.ch) or Ulrich K. Krieger (Ulrich.krieger@env.ethz.ch).

Acknowledgements. NB is grateful for support from the ETH Zurich Postdoctoral Fellowship program.

Competing interests. The authors declare that they have no conflict of interest.

References

Arnold, S., Amani, Y. and Orenstein, A.: Photophoretic spectrometer, Rev. Sci. Instrum., 51(9), 1202–1204, doi:10.1063/1.1136395, 1980.

Beresnev, S., Chernyak, V. and Fomyagin, G.: Photophoresis of a spherical particle in a rarefied gas, Phys. Fluids A, 5(8), 2043–2052, doi:10.1063/1.858540, 1992.

Birdsall, A. W., Krieger, U. K. and Keutsch, F. N.: Electrodynamic balance–mass spectrometry of single particles as a new platform for atmospheric chemistry research, Atmos. Meas. Tech., 11(1), 33–47, doi:10.5194/amt-11-33-2018, 2018.

Bluvshtein, N., Michel Flores, J., Segev, L. and Rudich, Y.: A new approach for retrieving the UV-vis optical properties of ambient aerosols, Atmos. Meas. Tech., 9(8), 3477–3490, doi:10.5194/amt-9-3477-2016, 2016.

Bohren, C. F.: Absorption and scattering of light by small particles, John Wiley & sons, INC, United States of America., 1983.

Bond, T. C., Doherty, S. J., Fahey, D. W., Forster, P. M., Berntsen, T., DeAngelo, B. J., Flanner, M. G., Ghan, S., Karcher, B., Koch, D., Kinne, S., Kondo, Y., Quinn, P. K., Sarofim, M. C., Schultz, M. G., Schulz, M., Venkataraman, C., Zhang, H., Zhang, S., Bellouin, N., Guttikunda, S. K., Hopke, P. K., Jacobson, M. Z., Kaiser, J. W., Klimont, Z., Lohmann, U., Schwarz,

J. P., Shindell, D., Storelvmo, T., Warren, S. G., Zender, C. S., Kärcher, B., Koch, D., Kinne, S., Kondo, Y., Quinn, P. K., Sarofim, M. C., Schultz, M. G., Schulz, M., Venkataraman, C., Zhang, H., Zhang, S., Bellouin, N., Guttikunda, S. K., Hopke, P. K., Jacobson, M. Z., Kaiser, J. W., Klimont, Z., Lohmann, U., Schwarz, J. P., Shindell, D., Storelvmo, T., Warren, S. G. and Zender, C. S.: Bounding the role of black carbon in the climate system: A scientific assessment, J. Geophys. Res. Atmos., 118(11), 5380–5552, doi:10.1002/jgrd.50171, 2013.

Brown, H., Liu, X., Feng, Y., Jiang, Y., Wu, M., Lu, Z., Wu, C., Murphy, S. and Pokhrel, R.: Radiative effect and climate impacts of brown carbon with the Community Atmosphere Model (CAM5), Atmos. Chem. Phys., 18(24), 17745–17768, doi:10.5194/acp-18-17745-2018, 2018.

Chen, Y. and Bond, T. C.: Light absorption by organic carbon from wood combustion, Atmos. Chem. Phys., 10(4), 1773–1787, doi:DOI 10.5194/acp-10-1773-2010, 2010.

Colberg, C. A., Krieger, U. K. and Peter, T.: Morphological Investigations of Single Levitated H2SO 4/NH3/H2O Aerosol Particles during Deliquescence/Efflorescence Experiments, J. Phys. Chem. A, 108(14), 2700–2709, doi:10.1021/jp037628r, 2004.

Dasari, S., Andersson, A., Bikkina, S., Holmstrand, H., Budhavant, K., Satheesh, S., Asmi, E., Kesti, J., Backman, J., Salam, A., Bisht, D. S., Tiwari, S., Hameed, Z. and Gustafsson, Ö.: Photochemical degradation affects the light absorption of water-soluble brown carbon in the South Asian outflow, Sci. Adv., 5(1), eaau8066, doi:10.1126/sciadv.aau8066, 2019.

Davis, E. J., Buehler, M. F. and Ward, T. L.: The double-ring electrodynamic balance for microparticle characterization, Rev. Sci. Instrum., 61(4), 1281–1288, doi:10.1063/1.1141227, 1990.

Drozd, G. T. and McNeill, V. F.: Organic matrix effects on the formation of light-absorbing compounds from α-dicarbonyls in aqueous salt solution, Environ. Sci. Process. Impacts, 16(4), 741–747, doi:10.1039/C3EM00579H, 2014.

Feng, Y., Ramanathan, V. and Kotamarthi, V. R.: Brown carbon: A significant atmospheric absorber of solar radiation, Atmos. Chem. Phys., 13(17), 8607–8621, doi:10.5194/acp-13-8607-2013, 2013.

Flores, J. M., Washenfelder, R. A., Adler, G., Lee, H. J., Segev, L., Laskin, J., Laskin, A., Nizkorodov, S. A., Brown, S. S. and Rudich, Y.: Complex refractive indices in the near-ultraviolet spectral region of biogenic secondary organic aerosol aged with ammonia, Phys. Chem. Chem. Phys., 16(22), 10629–10642, doi:10.1039/c4cp01009d, 2014a.

Flores, J. M., Zhao, D. F., Segev, L., Schlag, P., Kiendler-Scharr, A., Fuchs, H., Watne, A. K., Bluvshtein, N., Mentel, T. F., Hallquist, M. and Rudich, Y.: Evolution of the complex refractive index in the UV spectral region in ageing secondary organic aerosol, Atmos. Chem. Phys., 14(11), 5793–5806, doi:10.5194/acp-14-5793-2014, 2014b.

Francesconi, R., Bigi, A., Rubini, K. and Comelli, F.: Molar Heat Capacities, Densities, Viscosities, and Refractive Indices of Poly(ethylene glycols) + 2-Methyltetrahydrofuran at (293.15, 303.15, and 313.15) K, J. Chem. Eng. Data, 52(5), 2020–2025, doi:10.1021/je7003066, 2007.

Ganta, D., Dale, E. B., Rezac, J. P. and Rosenberger, A. T.: Optical method for measuring thermal accommodation coefficients using a whispering-gallery microresonator, J. Chem. Phys., 135(8), 084313, doi:10.1063/1.3631342, 2011.

Han, F., Zhang, J., Chen, G. and Wei, X.: Density, Viscosity, and Excess Properties for Aqueous Poly(ethylene glycol)

Solutions from (298.15 to 323.15) K, J. Chem. Eng. Data, 53(11), 2598–2601, doi:10.1021/je800464t, 2008.

He, Q. F., Bluvshtein, N., Segev, L., Meidan, D., Flores, J. M., Brown, S. S., Brune, W. and Rudich, Y.: Evolution of the Complex Refractive Index of Secondary Organic Aerosols during Atmospheric Aging, Environ. Sci. Technol., 52(6), 3456–3465, doi:10.1021/acs.est.7b05742, 2018.

Hems, R. F. and Abbatt, J. P. D.: Aqueous Phase Photo-oxidation of Brown Carbon Nitrophenols: Reaction Kinetics, Mechanism, and Evolution of Light Absorption, ACS Earth Sp. Chem., 2(3), 225–234, doi:10.1021/acsearthspacechem.7b00123, 2018.

Hoffer, A., Kiss, G., Blazso, M. and Gelencser, A.: Chemical characterization of humic-like substances (HULIS) formed from a lignin-type precursor in model cloud water, Geophys. Res. Lett., 31(6), doi:10.1029/2003gl018962, 2004.

Hovenier, M. I. M. J. W.: Light Scattering by Nonspherical Particles: Theory, Measurements, and Applications, Meas. Sci. Technol., 11(12), 1827, doi:10.1088/0957-0233/11/12/705, 2000.

Ivchenko, I. N., Loyalka, S. K. and Tompson, R. V.: A boundary model for the thermal creep problem, Fluid Dyn., 28(6), 876–878, doi:10.1007/BF01049795, 1993.

Jørgensen, K. and Skibsted, L. H.: Light sensitivity of cochineal. Quantum yields for photodegradation of carminic acid and conjugate bases in aqueous solution, Food Chem., 40(1), 25–34, doi:10.1016/0308-8146(91)90016-H, 1991.

Kanakidou, M., Seinfeld, J. H., Pandis, S. N., Barnes, I., Dentener, F. J., Facchini, M. C., Van Dingenen, R., Ervens, B., Nenes, A., Nielsen, C. J., Swietlicki, E., Putaud, J. P., Balkanski, Y., Fuzzi, S., Horth, J., Moortgat, G. K., Winterhalter, R., Myhre, C. E. L., Tsigaridis, K., Vignati, E., Stephanou, E. G. and Wilson, J.: Organic aerosol and global climate modelling: a review, Atmos. Chem. Phys., 5, 1053–1123, doi:DOI 10.5194/acp-5-1053-2005, 2005.

Kaskaoutis, D. G., Kambezidis, H. D., Hatzianastassiou, N., Kosmopoulos, P. G. and Badarinath, K. V. S.: Aerosol climatology: dependence of the Angstrom exponent on wavelength over four AERONET sites, Atmos. Chem. Phys. Discuss., 7(3), 7347–7397, doi:10.5194/acpd-7-7347-2007, 2007.

Kim, J. H., Mulholland, G. W., Kukuck, S. R. and Pui, D. Y. H.: Slip correction measurements of certified PSL nanoparticles using a nanometer differential mobility analyzer (Nano-DMA) for knudsen number from 0.5 to 83, J. Res. Natl. Inst. Stand. Technol., 110(1), 31–54, doi:10.6028/jres.110.005, 2005.

Kirchstetter, T. W., Novakov, T. and Hobbs, P. V: Evidence that the spectral dependence of light absorption by aerosols is affected by organic carbon, J. Geophys. Res., 109(D21), doi:10.1029/2004jd004999, 2004.

Krieger, U. K., Colberg, C. A., Weers, U., Koop, T. and Peter, T.: Supercooling of single H2SO4/H2O aerosols to 158 K: No evidence for the occurrence of the octrahydrate, Geophys. Res. Lett., 27(14), 2097–2100, doi:10.1029/2000GL011613, 2000.

Lack, D. A. and Cappa, C. D.: Impact of brown and clear carbon on light absorption enhancement, single scatter albedo and absorption wavelength dependence of black carbon, Atmos. Chem. Phys., 10(9), 4207–4220, doi:10.5194/acp-10-4207-2010, 2010.

Lack, D. A., Richardson, M. S., Law, D., Langridge, J. M., Cappa, C. D., McLaughlin, R. J. and Murphy, D. M.: Aircraft Instrument for Comprehensive Characterization of Aerosol Optical Properties, Part 2: Black and Brown Carbon Absorption

and Absorption Enhancement Measured with Photo Acoustic Spectroscopy, Aerosol Sci. Technol., 46(5), 555–568, doi:10.1080/02786826.2011.645955, 2012a.

Lack, D. A., Langridge, J. M., Bahreini, R., Cappa, C. D., Middlebrook, A. M. and Schwarz, J. P.: Brown carbon and internal mixing in biomass burning particles, Proc. Natl. Acad. Sci. U. S. A., 109(37), 14802–14807, doi:10.1073/pnas.1206575109, 2012b.

Lam, C. C., Leung, P. T. and Young, K.: Explicit asymptotic formulas for the positions, widths, and strengths of resonances in Mie scattering, J. Opt. Soc. Am. B, 9(9), 1585, doi:10.1364/josab.9.001585, 1992.

Lambe, A. T., Cappa, C. D., Massoli, P., Onasch, T. B., Forestieri, S. D., Martin, A. T., Cummings, M. J., Croasdale, D. R., Brune, W. H., Worsnop, D. R. and Davidovits, P.: Relationship between oxidation level and optical properties of secondary organic aerosol, Environ. Sci. Technol., 47(12), 6349–6357, doi:10.1021/es401043j, 2013.

Laskin, A., Laskin, J. and Nizkorodov, S. A.: Chemistry of Atmospheric Brown Carbon, Chem. Rev., 115(10), 4335–4382, doi:10.1021/cr5006167, 2015.

Latini, G., Di Nicola, G. and Pierantozzi, M.: A critical survey of thermal conductivity literature data for organic compounds at atmospheric pressure and an equation for aromatic compounds, in Energy Procedia, vol. 45, pp. 616–625, Elsevier Ltd., 2014.

Lavi, A., Bluvshtein, N., Segre, E., Segev, L., Flores, M. and Rudich, Y.: Thermochemical, Cloud Condensation Nucleation Ability, and Optical Properties of Alkyl Aminium Sulfate Aerosols, J. Phys. Chem. C, 117(43), 22412–22421, doi:10.1021/jp403180s, 2013.

Lee, A. K. Y., Zhao, R., Li, R., Liggio, J., Li, S.-M. and Abbatt, J. P. D.: Formation of Light Absorbing Organo-Nitrogen Species from Evaporation of Droplets Containing Glyoxal and Ammonium Sulfate, Environ. Sci. Technol., 47(22), 12819–12826, doi:10.1021/es402687w, 2013.

Lee, H. J., Aiona, P. K., Laskin, A., Laskin, J. and Nizkorodov, S. A.: Effect of Solar Radiation on the Optical Properties and Molecular Composition of Laboratory Proxies of Atmospheric Brown Carbon, Environ. Sci. Technol., 48(17), 10217–10226, doi:10.1021/es502515r, 2014.

Li, Y. Q., Davidovits, P., Shi, Q., Jayne, T., Kolb, C. E. and Worsnop, D. R.: Mass and thermal accommodation coefficients of h2o(g) on liquid water as a function of temperature, J. Phys. Chem. A, 105(47), 10632–10634, doi:10.1021/jp012758q, 2001.

Liu, P., Zhang, Y. and Martin, S. T.: Complex Refractive Indices of Thin Films of Secondary Organic Materials by Spectroscopic Ellipsometry from 220 to 1200 nm, Environ. Sci. Technol., 47(23), 13594–13601, doi:10.1021/es403411e, 2013.

Liu, S., Shilling, J. E., Song, C., Hiranuma, N., Zaveri, R. A. and Russell, L. M.: Hydrolysis of Organonitrate Functional Groups in Aerosol Particles, Aerosol Sci. Technol., 46(12), 1359–1369, doi:10.1080/02786826.2012.716175, 2012.

Lockerby, D. A., Reese, J. M., Emerson, D. R. and Barber, R. W.: Velocity boundary condition at solid walls in rarefied gas calculations, Phys. Rev. E - Stat. Physics, Plasmas, Fluids, Relat. Interdiscip. Top., 70(1), 4,

doi:10.1103/PhysRevE.70.017303, 2004.

Loyalka, S. K.: Momentum and temperature-slip coefficients with arbitrary accommodation at the surface, J. Chem. Phys., 48(12), 5432–5436, doi:10.1063/1.1668235, 1968.

Mackowski, D. W.: Photophoresis of aerosol particles in the free molecular and slip-flow regimes, Int. J. Heat Mass Transf., 32(5), 843–854, doi:10.1016/0017-9310(89)90233-0, 1989.

Marcos, M. A., Cabaleiro, D., Guimarey, M. J. G., Comuñas, M. J. P., Fedele, L., Fernández, J. and Lugo, L.: PEG 400-based phase change materials nano-enhanced with functionalized graphene nanoplatelets, Nanomaterials, 8(1), doi:10.3390/nano8010016, 2018.

Marrero-Ortiz, W., Hu, M., Du, Z., Ji, Y., Wang, Y., Guo, S., Lin, Y., Gomez-Hermandez, M., Peng, J., Li, Y., Secrest, J., Zamora, M. L., Wang, Y., An, T. and Zhang, R.: Formation and Optical Properties of Brown Carbon from Small α-Dicarbonyls and Amines, Environ. Sci. Technol., 53(1), 117–126, doi:10.1021/acs.est.8b03995, 2019.

Matzler, C.: Matlab codes foe mie scattering and absorption, , 13, 125–128, 2002.

Moosmuller, H., Chakrabarty, R. K., Ehlers, K. M. and Arnott, W. P.: Absorption Angstrom coefficient, brown carbon, and aerosols: basic concepts, bulk matter, and spherical particles, Atmos. Chem. Phys., 11(3), 1217–1225, doi:10.5194/acp-11-1217-2011, 2011.

Myhre, G., Samset, B. H., Schulz, M., Balkanski, Y., Bauer, S., Berntsen, T. K., Bian, H., Bellouin, N., Chin, M., Diehl, T., Easter, R. C., Feichter, J., Ghan, S. J., Hauglustaine, D., Iversen, T., Kinne, S., Kirkevåg, A., Lamarque, J. F., Lin, G., Liu, X., Lund, M. T., Luo, G., Ma, X., van Noije, T., Penner, J. E., Rasch, P. J., Ruiz, A., Seland, Ø., Skeie, R. B., Stier, P., Takemura, T., Tsigaridis, K., Wang, P., Wang, Z., Xu, L., Yu, H., Yu, F., Yoon, J. H., Zhang, K., Zhang, H. and Zhou, C.: Radiative forcing of the direct aerosol effect from AeroCom Phase II simulations, Atmos. Chem. Phys., 13(4), 1853–1877, doi:10.5194/acp-13-1853-2013, 2013.

Nakayama, T., Matsumi, Y., Sato, K., Imamura, T., Yamazaki, A. and Uchiyama, A.: Laboratory studies on optical properties of secondary organic aerosols generated during the photooxidation of toluene and the ozonolysis of α-pinene, J. Geophys. Res., 115(D24), 11 PP, doi:10.1029/2010jd014387, 2010.

Nakayama, T., Sato, K., Matsumi, Y., Imamura, T., Yamazaki, A. and Uchiyama, A.: Wavelength and NOx dependent complex refractive index of SOAs generated from the photooxidation of toluene, Atmos. Chem. Phys., 13(2), 531–545, doi:10.5194/acp-13-531-2013, 2013.

Nguyen, T. B., Lee, P. B., Updyke, K. M., Bones, D. L., Laskin, J., Laskin, A. and Nizkorodov, S. A.: Formation of nitrogen- and sulfur-containing light-absorbing compounds accelerated by evaporation of water from secondary organic aerosols, J. Geophys. Res. Atmos., 117(D1), doi:10.1029/2011jd016944, 2012.

Nozière, B. and Córdova, A.: A Kinetic and Mechanistic Study of the Amino Acid Catalyzed Aldol Condensation of Acetaldehyde in Aqueous and Salt Solutions, J. Phys. Chem. A, 112(13), 2827–2837, doi:10.1021/jp7096845, 2008.

Nozière, B., Dziedzic, P. and Córdova, A.: Inorganic ammonium salts and carbonate salts are efficient catalysts for aldol condensation in atmospheric aerosols, Phys. Chem. Chem. Phys., 12(15), 3864–3872, doi:10.1039/B924443C, 2010.

Ofner, J., Krüger, H. U., Grothe, H., Schmitt-Kopplin, P., Whitmore, K. and Zetzsch, C.: Physico-chemical characterization of SOA derived from catechol and guaiacol – a model substance for the aromatic fraction of atmospheric HULIS, Atmos. Chem. Phys., 11(1), 1–15, doi:10.5194/acp-11-1-2011, 2011.

Pope, M., Arnold, S. and Rozenshtein, L.: Photophoretic spectroscopy, Chem. Phys. Lett., 62(3), 589–591, doi:10.1016/0009-2614(79)80770-8, 1979.

Powelson, M. H., Espelien, B. M., Hawkins, L. N., Galloway, M. M. and De Haan, D. O.: Brown Carbon Formation by Aqueous-Phase Carbonyl Compound Reactions with Amines and Ammonium Sulfate, Environ. Sci. Technol., 48(2), 985–993, doi:10.1021/es4038325, 2014.

Preston, T. C. and Reid, J. P.: Accurate and efficient determination of the radius, refractive index, and dispersion of weakly absorbing spherical particle using whispering gallery modes, J. Opt. Soc. Am. B, 30(8), 2113, doi:10.1364/josab.30.002113, 2013.

Preston, T. C. and Reid, J. P.: Determining the size and refractive index of microspheres using the mode assignments from Mie resonances, J. Opt. Soc. Am. A, 32(11), 2210, doi:10.1364/josaa.32.002210, 2015.

Reed, L. D.: Low Knudsen number photophoresis, J. Aerosol Sci., 8(2), 123–131, doi:10.1016/0021-8502(77)90073-8, 1977.

Reyes, C. A., Medina, M., Crespo-Hernandez, C., Cedeno, M. Z., Arce, R., Rosario, O., Steffenson, D. M., Ivanov, I. N., Sigman, M. E. and Dabestani, R.: Photochemistry of pyrene on unactivated and activated silica surfaces, Environ. Sci. Technol., 34(3), 415–421, doi:10.1021/es9905391, 2000.

Rohatschek, H.: Semi-empirical model of photophoretic forces for the entire range of pressures, J. Aerosol Sci., 26(5), 717–734, doi:10.1016/0021-8502(95)00011-Z, 1995.

Romonosky, D. E., Laskin, A., Laskin, J. and Nizkorodov, S. A.: High-Resolution Mass Spectrometry and Molecular Characterization of Aqueous Photochemistry Products of Common Types of Secondary Organic Aerosols, J. Phys. Chem. A, 119(11), 2594–2606, doi:10.1021/jp509476r, 2015.

Saleh, R., Robinson, E. S., Tkacik, D. S., Ahern, A. T., Liu, S., Aiken, A. C., Sullivan, R. C., Presto, A. A., Dubey, M. K., Yokelson, R. J., Donahue, N. M. and Robinson, A. L.: Brownness of organics in aerosols from biomass burning linked to their black carbon content, Nat. Geosci., 7(9), 647–650, doi:10.1038/NGEO2220, 2014.

Schnitzler, E. G. and Abbatt, J. P. D.: Heterogeneous OH oxidation of secondary brown carbon aerosol, Atmos. Chem. Phys., 18(19), 14539–14553, doi:10.5194/acp-18-14539-2018, 2018.

Shaw, R. A. and Lamb, D.: Experimental determination of the thermal accommodation and condensation coefficients of water, J. Chem. Phys., 111(23), 10659–10663, doi:10.1063/1.480419, 1999.

Soong, C.-Y., Li, W.-K., Liu, C.-H. and Tzeng, P.-Y.: Effect of thermal stress slip on microparticle photophoresis in gaseous media, Opt. Lett., 35(5), 625, doi:10.1364/ol.35.000625, 2010.

Steimer, S. S., Krieger, U. K., Te, Y. F., Lienhard, D. M., Huisman, A. J., Luo, B. P., Ammann, M. and Peter, T.: Electrodynamic balance measurements of thermodynamic, kinetic, and optical aerosol properties inaccessible to bulk methods, Atmos. Meas. Tech., 8(6), 2397–2408, doi:10.5194/amt-8-2397-2015, 2015.

Sun, H. L., Biedermann, L. and Bond, T. C.: Color of brown carbon: A model for ultraviolet and visible light absorption by organic carbon aerosol, Geophys. Res. Lett., 34(17), doi:Artn L17813 Doi 10.1029/2007gl029797, 2007.

Tang, I. N. and Munkelwitz, H. R.: Water activities, densities, and refractive indices of aqueous sulfates and sodium nitrate droplets of atmospheric importance, J. Geophys. Res. Atmos., 99(D9), 18801–18808, doi:10.1029/94jd01345, 1994.

Trainic, M., Riziq, A. A., Lavi, A., Flores, J. M. and Rudich, Y.: The optical, physical and chemical properties of the products of glyoxal uptake on ammonium sulfate seed aerosols, Atmos. Chem. Phys., 11(18), 9697–9707, doi:10.5194/acp-11-9697-2011, 2011.

Trott, W. M., Rader, D. J., Castañeda, J. N., Torczynski, J. R. and Gallis, M. A.: Experimental measurements of thermal accommodation coefficients for microscale gas-phase heat transfer, in Collection of Technical Papers - 39th AIAA Thermophysics Conference, vol. 1, pp. 233–244., 2007.

Updyke, K. M., Nguyen, T. B. and Nizkorodov, S. A.: Formation of brown carbon via reactions of ammonia with secondary organic aerosols from biogenic and anthropogenic precursors, Atmos. Environ., 63, 22–31, doi:10.1016/j.atmosenv.2012.09.012, 2012.

Washenfelder, R. A., Flores, J. M., Brock, C. A., Brown, S. S. and Rudich, Y.: Broadband measurements of aerosol extinction in the ultraviolet spectral region, Atmos. Meas. Tech. Discuss., 6(1), 113–157, doi:10.5194/amtd-6-113-2013, 2013.

Yalamov, Y. I., Kutukov, V. B. and Shchukin, E. R.: Theory of the photophoretic motion of the large-size volatile aerosol particle, J. Colloid Interface Sci., 57(3), 564–571, doi:10.1016/0021-9797(76)90234-4, 1976.

Zardini, A. A., Sjogren, S., Marcolli, C., Krieger, U. K., Gysel, M., Weingartner, E., Baltensperger, U. and Peter, T.: A combined particle trap/HTDMA hygroscopicity study of mixed inorganic/organic aerosol particles, Atmos. Chem. Phys., 8(18), 5589–5601, doi:10.5194/acp-8-5589-2008, 2008.

Zhang, Q., Jimenez, J. L., Canagaratna, M. R., Allan, J. D., Coe, H., Ulbrich, I., Alfarra, M. R., Takami, A., Middlebrook, A. M., Sun, Y. L., Dzepina, K., Dunlea, E., Docherty, K., DeCarlo, P. F., Salcedo, D., Onasch, T., Jayne, J. T., Miyoshi, T., Shimono, A., Hatakeyama, S., Takegawa, N., Kondo, Y., Schneider, J., Drewnick, F., Borrmann, S., Weimer, S., Demerjian, K., Williams, P., Bower, K., Bahreini, R., Cottrell, L., Griffin, R. J., Rautiainen, J., Sun, J. Y., Zhang, Y. M. and Worsnop, D. R.: Ubiquity and dominance of oxygenated species in organic aerosols in anthropogenically-influenced Northern Hemisphere midlatitudes, Geophys. Res. Lett., 34(13), doi:10.1029/2007gl029979, 2007.

Zhao, R., Lee, A. K. Y., Huang, L., Li, X., Yang, F. and Abbatt, J. P. D.: Photochemical processing of aqueous atmospheric brown carbon, Atmos. Chem. Phys., 15(11), 6087–6100, doi:10.5194/acp-15-6087-2015, 2015.

Zheng, G., He, K., Duan, F., Cheng, Y. and Ma, Y.: Measurement of humic-like substances in aerosols: A review, Environ. Pollut., 181, 301–314, doi:10.1016/j.envpol.2013.05.055, 2013.

Table 1: thermal conductivity (W m^{-1} K^{-1}) of organic compounds from Latini et al (2014) and references therein.

	Number of data sets	Mean value	Standard deviation	Standard deviation %
Alcohols	775	0.1482	0.0256	17.3
Alkanes	1025	0.1259	0.0182	14.5
Alkenes	135	0.1301	0.0244	18.7
Aromatics	570	0.1174	0.0180	15.3
Carboxylic acids	318	0.1576	0.0427	27.1
Cycloalkanes	35	0.1262	0.0134	10.6
Cycloalkenes	10	0.1303	0.0104	8.0
Esters	236	0.1261	0.0179	14.2
Ethers	111	0.1268	0.0181	14.3
Ketones	185	0.1417	0.0203	14.3

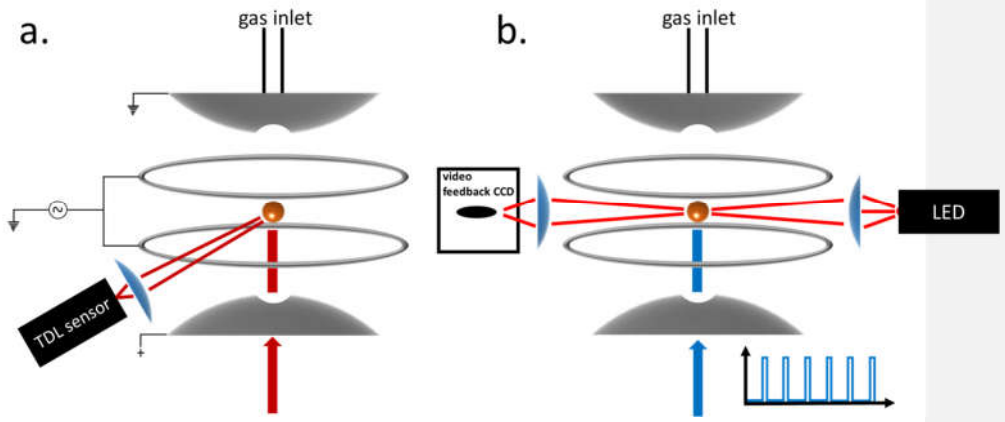

Figure 1: Schematic diagram of the experimental set up. (a) Measurement of high-resolution elastic light scattering at 900 by illuminating the particle with a 765–781 nm TDL. (b) Continuous illumination of the particle with a red light-emitting diode (LED) used for the active feedback adjustment of the DC voltage and alternating illumination with the 473 nm laser used to impose vertical optical forces on the particle.

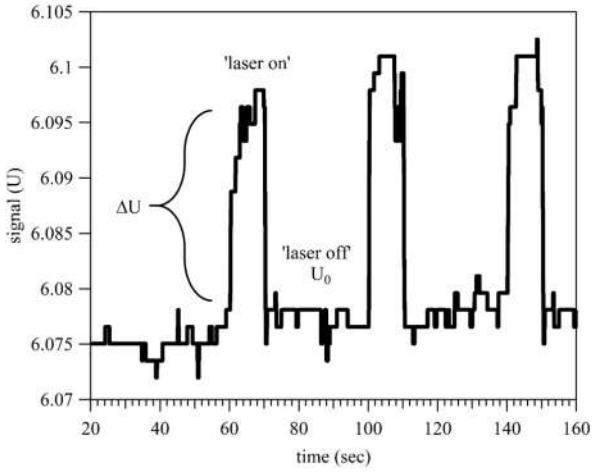

Figure 2: change in the applied DC voltage in response to alternately illuminating a trapped light absorbing particle. Here, a particle with 12.72 µm radius and $\kappa \approx 1.36 \times 10^{-4}$ was levitated in 400 mbar of dry nitrogen. For more details on how the particle size and imaginary part of the CRI where determined refer to section 2.2 and 3.

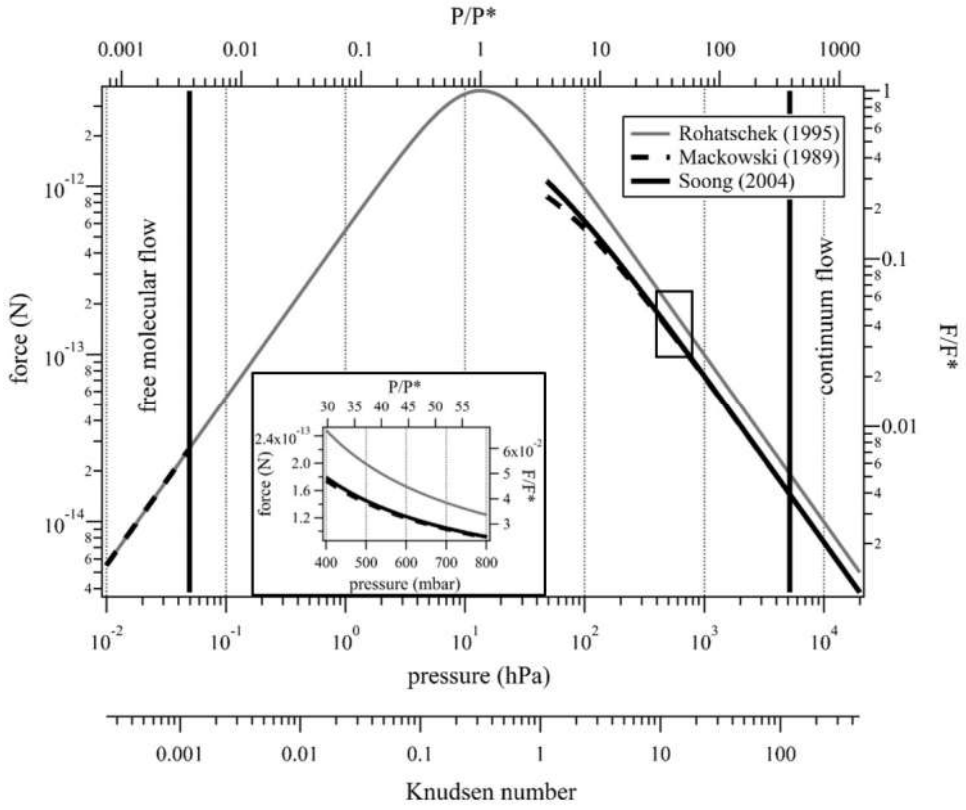

635 **Figure 3. Indirect photophoretic force calculated with the Rohatschek (1995) approximation at the full pressure range (gray line), Mackowski (1989) analytical solution (dashed line) and the Soong (2004) correction (solid line) for a slightly absorbing particle with radius of 10 µm, T = 20 ^{0}C, m = $1.466 + i10^{-4}$, λ = 473 nm, $I = 35$ mW mm^{-2} and full thermal accommodation. The black rectangle and the insert plot show the pressure range that is possible with our experimental system.**

Deleted: 2

Deleted: Knudsen number (red line) and the i

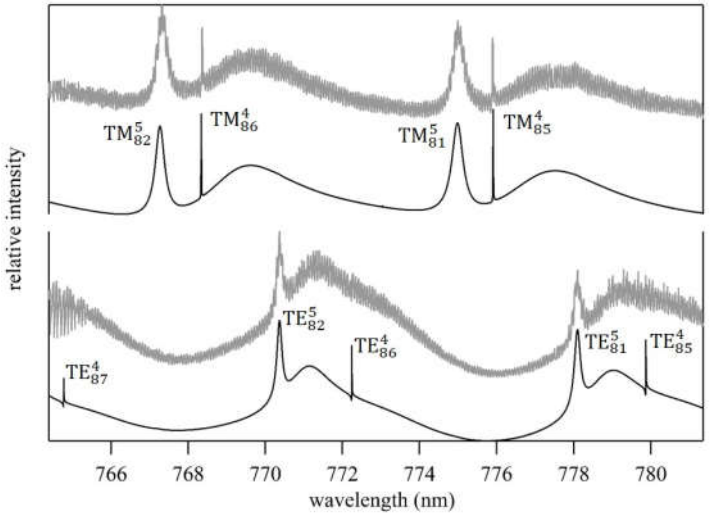

Figure 4. Measured Mie scattering spectra at $\pi/2$ angle of a levitated particle. The positions of the TE and TM resonance modes (e.g. TM^l_n; identified by their order (l) and mode (n) numbers) were used to retrieve the particle's real refractive index (n_D =1.4665, m_1 =2745) and size (a = 9.2906 µm). We note that the lower order modes in the fitted TE spectrum are too narrow to be observed in the measured spectrum with the current resolution. Residual noise in the measured spectrum originate mostly from laser power oscillations due to frequency scanning operation and from horizontal oscillation of the particle due to the applied AC field.

Deleted: 3

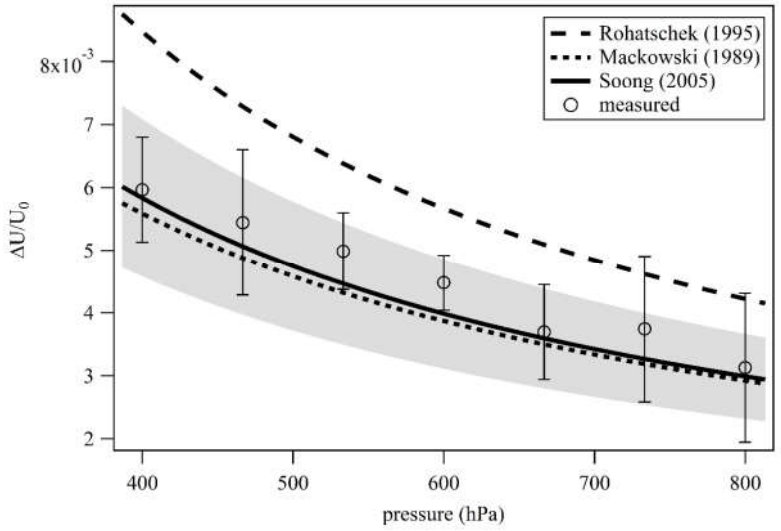

Figure 5. Measured and simulated EDB response ($\Delta U/U_0$) to the illumination of a slightly absorbing particle due to the photophoretic effect. The two analytical solutions; Mackowski (1989) dotted line and Soong et al. (2005) solid line that account for slip-flow conditions agree well with our measurements (empty circles). Error bars: standard deviation over five illumination cycles. Gray shaded area: measurement uncertainty propagated through the Soong model calculation, dominated by the 15% uncertainty on the radiant flux measured with a power meter and a beam profiler.

Deleted: 4

Deleted: line, that

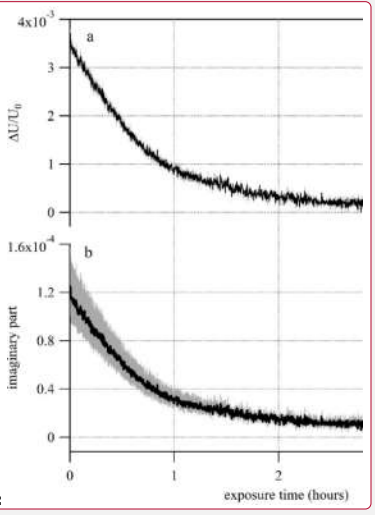

Deleted:

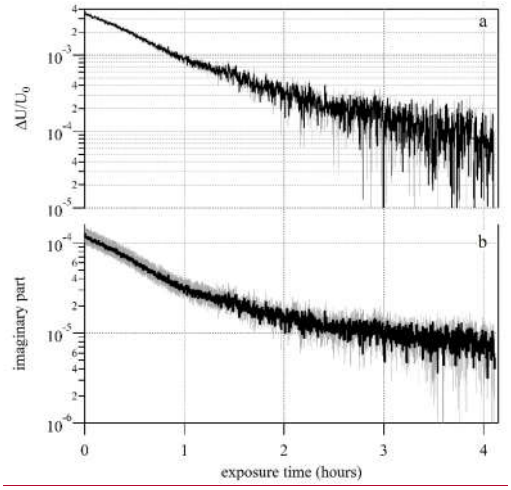

Figure 6. (a) Decay of the EDB photophoretic response ($\Delta U/U_0$) during illumination of a slightly absorbing particle (PEG400 with 0.23% wt of carminic acid; CA). The decay is due to the slow photolysis of the CA. (b) The retrieved imaginary part of the complex refractive index. Gray shaded area in both plots represents the uncertainty in the measured and retrieved values.

Deleted: 5

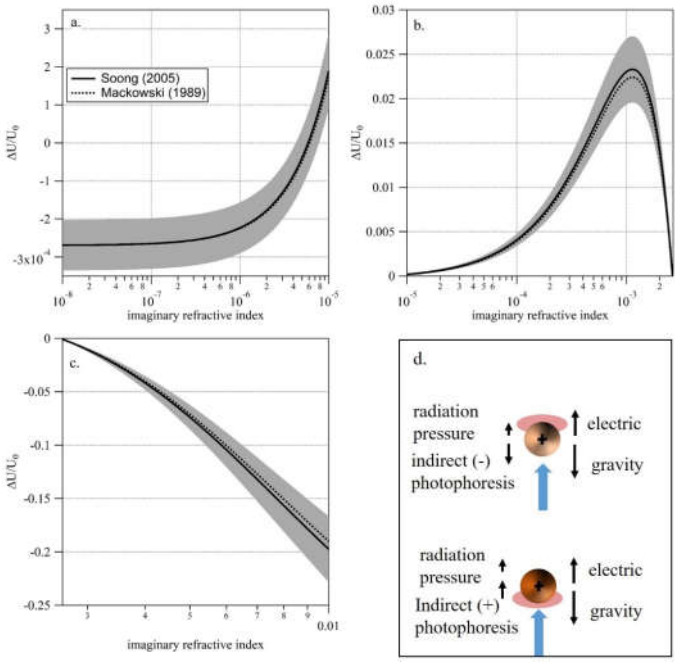

Figure 7: simulated signal (and uncertainty) for a PEG400 particle, 10 µm in radius at T = 20 ^{0}C, P = 400 mbar, $m_1 = 1.466$, $\lambda = 473$ nm, $I = 35$ mW mm^{-2} and full thermal accommodation with increasing imaginary part of the CRI. (a) Transition from negligible absorptivity and negative signal (i.e. dominated by radiation pressure) to positive signal (i.e. dominated by negative indirect photophoresis). (b) Increasing absorptivity leads to increasing positive asymmetry parameter and stronger positive signal (i.e. negative indirect photophoresis). Additional absorptivity leads to asymmetry parameter of zero as the surfaces of the upper and lower hemispheres of the particle are effectively at equal temperature. (c) Additional increase in absorptivity leads to an increase of a negative asymmetry parameter and stronger positive indirect photophoresis. (d) An illustration of the positive and negative indirect photophoresis regimes. Black arrows represent the various forces acting on a 'strongly' (lower) and 'slightly' (upper) absorbing particle when illuminated with the laser beam (blue arrow).